International Journal of Thermophysics, Vol. 21, No. 4, 2000

Application of Laser Polarimetry to the Measurement of Specific Heat Capacity and Enthalpy of the Alloy 53Nb–47Ti (mass%) in the Temperature Range 1600 to 2000 K by a Millisecond-Resolution Pulse Heating Technique

D. Basak,[1,2] U. R. Kattner,[1] J. L. McClure,[1] D. Josell,[1] and A. Cezairliyan[1,3]

Received November 4, 1999

The determination of the specific heat capacity, enthalpy, and electrical resistivity of the alloy 53Nb–47Ti (mass%) in the temperature range 1600 to 2000 K is described. The method is based on rapid resistive self-heating of a solid cylindrical specimen from room temperature to the maximum temperature of interest by the passage of a subsecond-duration electric current pulse through the specimen and on simultaneously measuring the pertinent experimental quantities. The experimental quantities measured are the current through the specimen, voltage drop across the effective specimen, specimen radiance temperature at two wavelengths, and normal spectral emissivity of the specimen. The present study extends this technique, previously applied to pure metals, to the determination of specific heat capacity and enthalpy of the alloy, 53Nb–47Ti. The measured properties were compared to those calculated from a thermodynamic description of the Nb–Ti system.

KEY WORDS: electrical resistivity; enthalpy; high temperature; laser polarimetry; Nb–Ti alloy; pulse heating; specific heat capacity.

1. INTRODUCTION

A millisecond-resolution pulse-heating technique [1, 2] has been extensively used for over 25 years at NIST for accurate measurements of thermophysical

[1] Metallurgy Division, National Institute of Standards and Technology, Gaithersburg, Maryland 20899, U.S.A.
[2] To whom correspondence should be addressed.
[3] Deceased.

0195-928X/00/0700-0913$18.00/0

properties of electrically conducting materials, particularly pure metals. Until recently, the specimen used in the experiments was in the form of a thin-wall tube with a small hole fabricated in the wall in the middle of the tube to approximate blackbody conditions for optical temperature measurements. Additional material was removed along the remaining length of the specimen to ensure that the cross-sectional area of the specimen was uniform over the length. Tubular geometry and precise fabrication requirements involved complex machining, which made specimen preparation time-consuming and expensive.

In 1992, an alternative method for true temperature measurement was developed that eliminates the need for a blackbody configuration of the specimen [3]. By simultaneously measuring the normal spectral emissivity by laser polarimetry and the surface radiance temperature by optical pyrometry, the true temperature of the specimen is determined using Planck's law with millisecond time resolution. To validate the accuracy of the laser polarimetry technique, simultaneous measurements were performed by the old and new techniques on specimens of molybdenum and tungsten. The average absolute difference in the measured normal spectral emissivity by the two techniques is about 0.3% for molybdenum and about 0.7% for tungsten [4]. Also, a comparison of the specific heat capacity data of Standard Reference Material (SRM) molybdenum [5] with those reported in the literature [6] shows that the agreement is good; the maximum deviation is 0.5%over the temperature range of the experiments, i.e., 2000 to 2800 K.

The present work extends the use of the laser polarimetry technique in conjunction with optical pyrometry to the determination of the specific heat capacity and enthalpy of the alloy 53Nb–47Ti (mass%). This alloy exhibits complete solubility of its components in the solid and liquid states. It was selected because of its simple "lens-shaped" phase diagram and its easy commercial availability. The enthalpy of the material was calculated from the specific heat capacity data. The electrical resistivity was determined from voltage and current measurements on the specimen. The experimentally determined specific heat capacity and enthalpy were compared with those determined from a thermodynamic description of the system, for mutual validation.

2. MEASUREMENT METHOD

The method is based on rapid resistive self-heating of the specimen from room temperature to high temperatures (up to near its melting point) of subsecond duration by the passage of an electric current pulse. During heating, the current through the specimen, the voltage drop across the

effective specimen (the length of the specimen between two knife-edge probes), the normal spectral emissivity of the specimen, and the radiance temperature of the specimen are measured with millisecond resolution. The current through the specimen is determined from the voltage drop across a standard resistor placed in series with the specimen. The normal spectral emissivity is measured with a high-speed laser polarimeter [3]. In this method, the normal spectral emissivity is determined by directing a modulated and polarized beam from a helium–neon laser ($\lambda = 633$ nm) to the specimen and analyzing the polarization state of the reflected beam. The surface radiance temperature of the specimen is measured at two wavelengths, 625 and 651 nm, by two high-speed solid-state optical pyrometers [7, 8], each focused on a region diametrically opposite to the other on the specimen surface. These two wavelengths bracket the operating wavelength of the laser source. The surface radiance temperature at 633 nm is calculated by linear interpolation of the surface radiance temperatures measured at the bracketing wavelengths of 625 and 651 nm. Using Planck's law, the true temperature of the specimen is then determined from the data on radiance temperature and normal spectral emissivity, both at 633 nm. Use of the interpolated radiance temperature at 633 nm rather than the actual value would result in an error of less than 1 K.

The high-speed digital data-acquisition system used in these experiments has a 16-bit resolution and can record data at a sampling rate of 2000 data points per s for each experimental quantity. The design of the original measurement system and the methods of measuring the experimental quantities are provided in earlier publications [1, 2]. Several improvements have been made to the original system. One significant improvement was the development of a high-speed solid-state switch, which can be programmed to send precise levels of current through the specimen [9]. This system was used along with a PID (proportional-integral-derivative) control program to hold the temperature of the specimen constant during the steady-state experiments. The hemispherical total emissivity of the specimen was determined from such steady-state experiments, which was used to compute the radiation loss from the specimen during heating.

3. MEASUREMENTS

Measurements were performed on a cylindrical specimen, the nominal dimensions of which were a length of 73 mm and a diameter of 1.6 mm. The mass percentage composition of this alloy has been confirmed in an analysis reported elsewhere [10]. The specimen was polished to a smooth finish (down to 600-grit silicon carbide paper) to provide good reflection characteristics for the laser beam and to minimize radiative power loss

somewhat. Before the experiments, the specimen was cleaned of surface contaminants and relieved of internal stresses by pulse-heating to 2085 K and holding it in vacuum at this temperature for 1 s.

Before conducting pulse experiments to determine the specific heat capacity of the alloy, several auxiliary steady-state experiments were conducted to provide data for the radiative power loss in the temperature range of interest. Because high-temperature exposure is limited to 1 s and only the central one-third of the specimen is considered as the effective specimen, conduction losses are not significant. During the steady-state period, the power input to the specimen is, therefore, equal to the power loss from the specimen due to thermal radiation. Accordingly, since power input equals power radiated,

$$EI = \varepsilon_T \sigma A_s (T^4 - T_0^4) \tag{1}$$

where E is the voltage across the effective specimen, I is the current through the specimen, ε_T is the hemispherical total emissivity, σ is the Stephan–Boltzmann constant, A_s is the surface area of the effective specimen, T is the specimen temperature, and T_0 is the ambient temperature. From Eq. (1), the hemispherical total emissivity of the specimen surface can be determined. Experiments were repeated at several temperatures in the range 1675 to 2025 K. Using the data so obtained, an expression for ε_T as a function of T is generated. This function is used to compute the radiative power loss from the specimen during the pulse experiments. This procedure has been described in detail in an earlier publication [9].

In the pulse experiments, the specimen was heated from room temperature to about 2000 K in less than 0.5 s, in an environment of argon (99.999% pure) slightly above atmospheric pressure. The average heating rate was 3000 $K \cdot s^{-1}$. The average current was 300 A.

Eight experimental quantities were recorded with a high-speed data acquisition system at increments of 0.5 ms during the pulse heating period. These quantities were the voltage drop across the standard resistor, the voltage drop across the effective specimen, the pyrometer outputs at 625- and 651-nm wavelengths, and four polarimeter outputs. The two pyrometer outputs yielded the radiance temperatures at the respective wavelengths. From the four polarimeter outputs, the normal spectral emissivity of the specimen was determined using a computer algorithm.

4. RESULTS

The details of the procedure for determining specific heat capacity from experimental data have been discussed in an earlier publication [1].

The specific heat capacity was obtained from the voltage, current, and temperature measurements during the pulse period by equating the power input to the specimen with the sum of the power absorbed and the power lost by radiation. For the two experiments, specific heat results in the temperature range 1600 to 2000 K were fitted to a second-order polynomial function of temperature. The function (standard deviation of 0.3%) that represents specific heat capacity results for the alloy in the temperature range 1600 to 2000 K is

$$C_p = 0.63982 - 3.0888 \times 10^{-4} T + 1.3692 \times 10^{-7} T^2 \quad (2)$$

where C_p is in $J \cdot g^{-1} \cdot K^{-1}$ and T is in K. Figure 1 shows the specific heat capacity data for the two experiments (each experiment represented with a different symbol) and the curve representing Eq. (2).

The equation for enthalpy versus temperature, Eq. (3), in the temperature range 1600 to 2000 K was obtained by analytically integrating the equation for specific heat capacity versus temperature, Eq. (2), in the same temperature range and adding to it the measured enthalpy at 1600 K. The measured enthalpy at 1600 K was determined by integrating the absorbed power with respect to time, from 298.15 K (reference temperature) to 1600 K. Radiative power losses were calculated from the Stephan–Boltzman law at each recorded temperature. Absorbed power was then calculated by subtracting the power lost from the power imparted. The function that

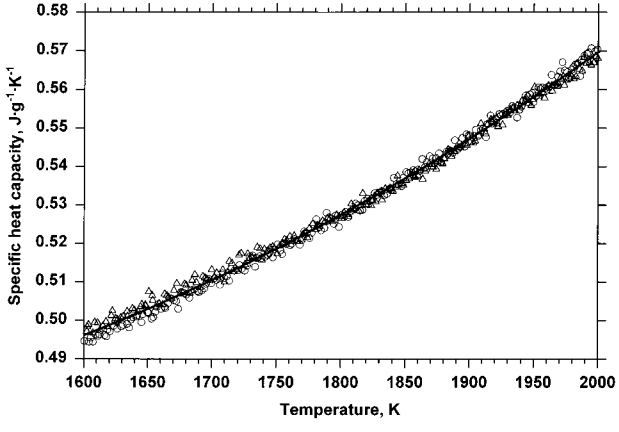

Fig. 1. Specific heat capacity of the alloy, 53Nb–47Ti. The symbols represent the two experiments, and the line represents the fit according to Eq. (2).

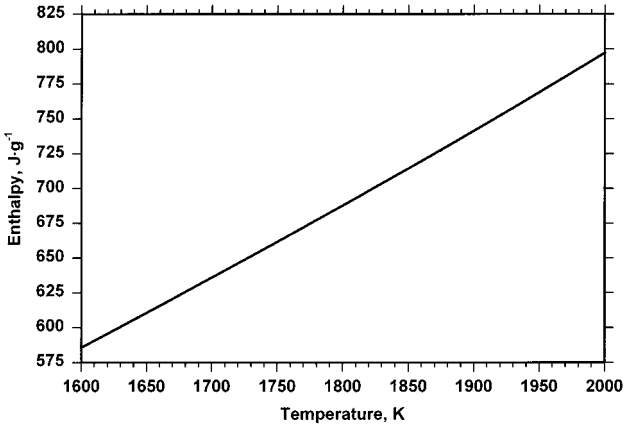

Fig. 2. Enthalpy of the alloy, 53Nb–47Ti, as represented by Eq. (3).

represents the enthalpy results for the alloy in the temperature range 1600 to 2000 K, based on a reference temperature of 298.15 K, is

$$H = -229.70 + 0.63982T - 1.5444 \times 10^{-4}T^2 + 4.5640 \times 10^{-8}T^3 \qquad (3)$$

where H is in $J \cdot g^{-1}$ and T is in K. Figure 2 shows the curve representing Eq. (3).

The electrical resistivity was calculated from the relation, $\rho = RA/L$, where ρ is the electrical resistivity of the specimen material, R is the specimen resistance across the voltage probes, A is the cross-sectional area of the specimen, which was measured with a precision micrometer at room temperature, and L is the length of the specimen between the voltage probes, which was measured with a traversing microscope. Electrical resistivity results over the temperature range 1600 to 2000 K for the two experiments were fitted to a second-order polynomial function. The function (standard deviation of 0.2%) that represents electrical resistivity results for the alloy in the temperature range 1600 to 2000 K is

$$\rho = 59.316 + 0.044618T - 5.8804 \times 10^{-6}T^2 \qquad (4)$$

where ρ is in $\mu\Omega \cdot$cm and T is in K. Figure 3 shows the electrical resistivity data for the two experiments (each experiment represented with a different symbol) and the curve representing Eq. (4). Electrical resistivity values are based on the room temperature dimensions of the specimen.

The specific heat capacity, enthalpy, and electrical resistivity of the alloy computed using Eqs. (2), (3), and (4), respectively, are given in Table I.

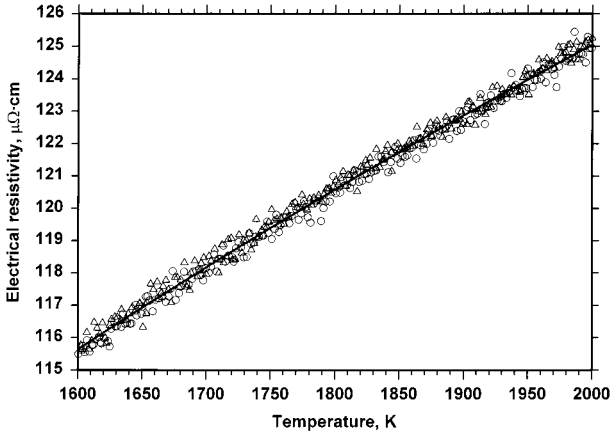

Fig. 3. Electrical resistivity of the alloy, 53Nb–47Ti. The symbols represent the two experiments, and the line represents the fit according to Eq. (4).

5. ESTIMATE OF UNCERTAINTIES

Sources of uncertainties in the measured experimental quantities and their magnitudes, evaluated around 2400 K, are reported in Table II. All uncertainties reported are at the 2-standard deviation level. The radiance temperature was measured with two pyrometers. Since both pyrometers are of similar design and operation, the uncertainty in the temperature measurements can be considered to be the same for both pyrometers. The main sources of temperature measurement uncertainty are the calibration

Table I. Specific Heat Capacity, Enthalpy, and Electrical Resistivity of the Alloy, 53Nb–47Ti, Determined from Experiments, in the Temperature Range 1600 to 2000 K

Temperature (K)	Specific heat capacity ($J \cdot g^{-1} \cdot K^{-1}$)	Enthalpy ($J \cdot g^{-1}$)	Electrical Resistivity ($\mu\Omega \cdot cm$)
1600	0.496	586	116
1650	0.503	611	117
1700	0.510	636	118
1750	0.519	662	119
1800	0.527	688	121
1850	0.537	714	122
1900	0.547	741	123
1950	0.558	769	124
2000	0.570	797	125

Table II. Relative Uncertainties in the Experimental Quantities and the Resultant Properties[a]

Quantity	Uncertainty ($\pm$%)[a]
Temperature (radiance)	0.2 (5 K)
Temperature (true)	0.3 (7 K)
Current	0.1
Voltage	0.1
Normal spectral emissivity (633 nm)	2
Specific heat capacity	3
Enthalpy	3
Electrical resistivity	1

[a] Two-standard deviation level.

uncertainty of the tungsten–filament lamp (secondary standard), alignment of the pyrometer with the specimen, and determination of the calibration constants of the pyrometers. The resultant total uncertainty in the measured radiance temperature obtained from the square root of the sum of the squares of the various individual uncertainties is about $\pm 0.2\%$ (5 K at 2400 K) between 625 and 651 nm. The main sources of polarimetric measurement uncertainty are the laser radiant flux measurements, instrument calibration, and estimation of the incidence angle. The uncertainty in the emissivity due to total uncertainties in the pertinent parameters was obtained from the square root of the sum of the squares of the individual uncertainties. The total uncertainty in emissivity from polarimetric measurements is $\pm 2\%$ at 633 nm. The uncertainties in the measurement of specimen length and mass have been estimated to be 0.04 and 0.01%, respectively and have been assumed to be negligible. Details about these uncertainty measurements have been discussed earlier [4]. It can be concluded that the resultant uncertainties in the properties are no more than $\pm 3\%$ for specific heat capacity, $\pm 3\%$ for enthalpy, and $\pm 1\%$ for electrical resistivity.

6. DISCUSSION

The laser-polarimetry technique for the determination of the true temperature of the specimen, which was demonstrated to work successfully for pure metals, was applied to the determination of the specific heat capacity and enthalpy of the alloy, 53Nb–47Ti. The same quantities, specific heat capacity and enthalpy, were also computed from a thermodynamic model of the alloy system. While the specific heat capacity data were in good agreement with the calculated values, the discrepancy in the enthalpy data compared to those calculated for the equilibrium condition ($\alpha + \beta$), led to

the recalculation of enthalpy values for the metastable ($\beta_1 + \beta_2$) and unstable (β) conditions. These considerations are discussed below.

The equilibrium phases in the Nb–Ti system are liquid, β [bcc-(Nb, Ti)], and α [hcp-(Ti)]. The most recent analytical description of the Gibbs energy of the phases in this system as a function of temperature and concentration was developed by Hari Kumar et al. [11]. All three phases were described as regular solutions, i.e., temperature-independent interaction parameters were used. The quantities for the pure elements were taken from Dinsdale [12]. The Gibbs energy functions can be used to calculate the phase diagram by minimizing the total Gibbs energy of the system or to calculate the thermochemical properties of the phases from the relations,

$$H = G - \frac{\partial G}{\partial T}\, T \tag{5}$$

$$C_p = \frac{\partial H}{\partial T} = -\frac{\partial^2 G}{\partial T^2}\, T \tag{6}$$

The calculated equilibrium phases for the 53Nb–47Ti alloy are α and β at temperatures below 777 K and single-phase β between 777 and 2118 K. The solidus and liquidus temperatures of the alloy are 2118 and 2191 K, respectively [10]. It should be noted that the β phase exhibits a metastable miscibility gap and that, if the α phase is not formed, two β phases would exist at temperatures below 522 K.

The expression for the specific heat capacity of the β phase obtained from Hari Kumar et al. consists only of the contributions of the pure elements,

$$C_p^{\beta} = x_{\mathrm{Nb}} C_{p\mathrm{Nb}}^{\beta 0} + x_{\mathrm{Ti}} C_{p\mathrm{Ti}}^{\beta 0} \tag{7}$$

while the expression for the enthalpy of the β phase also includes a regular solution interaction term,

$$H^{\beta} = x_{\mathrm{Nb}} H_{\mathrm{Nb}}^{\beta 0} + x_{\mathrm{Ti}} H_{\mathrm{Ti}}^{\beta 0} + x_{\mathrm{Nb}} x_{\mathrm{Ti}} L_{\mathrm{NbTi}}^{\beta} \tag{8}$$

where x_{Nb} and x_{Ti} are the molar fractions of Nb and Ti, $C_{p\mathrm{Nb}}^{\beta 0}$ and $C_{p\mathrm{Ti}}^{\beta 0}$ are the specific heat capacities, and $H_{\mathrm{Nb}}^{\beta 0}$ and $H_{\mathrm{Ti}}^{\beta 0}$ are the enthalpies, respectively, of the pure elements in the β phase. $L_{\mathrm{NbTi}}^{\beta}$ is the regular solution interaction term, which is temperature independent. To arrive at the enthalpy with respect to a reference state, the enthalpy of the alloy at the reference temperature of 298.15 K has to be subtracted, i.e., $H = H^{\beta} - H_{298.15}$.

A comparison of the experimentally determined specific heat capacity, Eq. (2), with that calculated from the quantities for the constituent

Table III. Experimental and Calculated Values for Enthalpy and Specific Heat Capacity of the Alloy, 53Nb–47Ti, in the Temperature Range 1600 to 2000 K

	Enthalpy ($J \cdot g^{-1}$)				Specific heat capacity ($J \cdot g^{-1} \cdot K^{-1}$)	
		Calculated				
Temperature (K)	Experimental	Equilibrium ($\alpha + \beta$)	Metastable ($\beta 1 + \beta 2$)	Unstable (β)	Experimental	Calculated
1600	586	668	601	573	0.496	0.502
1625	598	681	613	586	0.499	0.506
1650	611	694	626	598	0.503	0.510
1675	623	706	639	611	0.507	0.514
1700	636	719	652	624	0.510	0.518
1725	649	732	665	637	0.514	0.522
1750	662	745	678	650	0.519	0.526
1775	675	759	691	663	0.523	0.531
1800	688	772	704	677	0.527	0.535
1825	701	785	718	690	0.532	0.540
1850	714	799	731	704	0.537	0.545
1875	728	813	745	717	0.542	0.550
1900	741	826	759	731	0.547	0.554
1925	755	840	773	745	0.553	0.559
1950	769	854	787	759	0.558	0.564
1975	783	869	801	773	0.564	0.569
2000	797	883	815	788	0.570	0.574

elements, Eq. (7), in the temperature range 1600 to 2000 K is presented in Table III and shown in Fig. 4. Although the calculated specific heat capacity is about 1% higher than the experimentally determined quantity, the deviation is smaller than the estimated uncertainty of the measured quantity (Table II), and therefore, the introduction of an excess term for the specific heat capacity is not warranted.

The enthalpy for the following initial conditions—equilibrium ($\alpha + \beta$), metastable ($\beta_1 + \beta_2$), and unstable (β)—are presented in Table III and plotted in Fig. 5, along with the experimental data. To arrive at the enthalpy for the initial condition, equilibrium ($\alpha + \beta$), the value of $H_{298.15}$ was calculated for the stable two-phase equilibrium, $\alpha + \beta$, and subtracted from H^{β}. There is a rather large discrepancy (10 to 14%) between the calculated equilibrium values and the experimental values. It should be noted that, due to the lack of reliable thermochemical data, Hari Kumar et al. had to rely solely on the phase diagram data to determine the value of the regular solution parameter. Therefore, it may be concluded that this value needs to be readjusted. On the other hand, it is known that the $\beta \rightarrow \alpha$

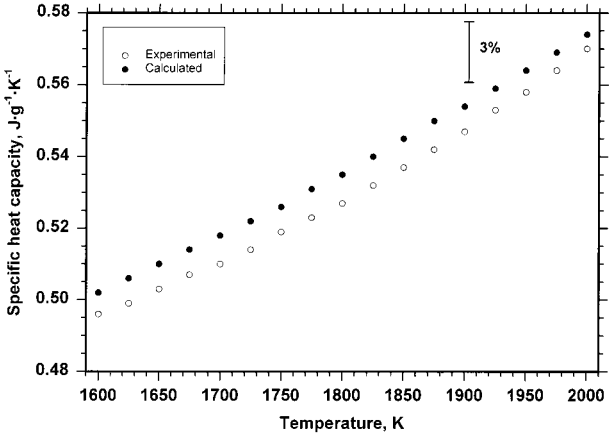

Fig. 4. Experimental values and the values calculated from thermodynamic model, for the specific heat capacity of the alloy, 53Nb–47Ti. The error bars indicate the estimated uncertainty of the experimental values at a 2-standard deviation level.

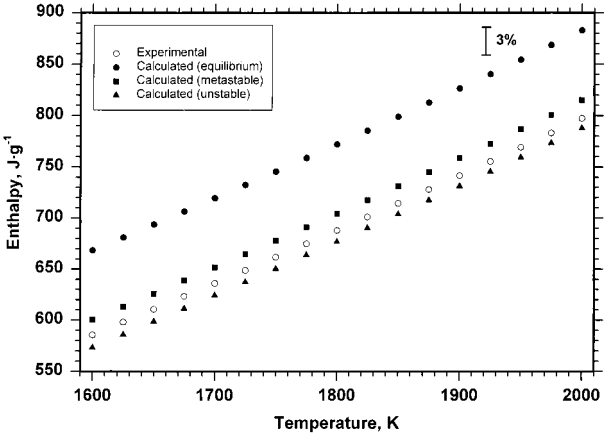

Fig. 5. Experimental values and values calculated from the thermodynamic model, for the three initial conditions, e.g., equilibrium, metastable, and unstable, for the enthalpy of the alloy, 53Nb–47Ti. The error bars indicate the estimated uncertainty of the experimental values at a 2-standard deviation level.

transformation is sluggish and that equilibrium is attained only after prolonged heat treatment [13]. Before the experiments, the specimen was pulse heated to 2085 K, held for 1 s, and then allowed to cool naturally. This was done to relieve internal strain and remove any oxide from the surface. It is likely that equilibrium at 298.15 K was not reached after the short-duration high-temperature heat treatment. Therefore, the enthalpies were also calculated with values of $H_{298.15}$ for metastable two-phase, $\beta_1 + \beta_2$, and for unstable single-phase β. The calculated values obtained for metastable two-phase, $\beta_1 + \beta_2$, are slightly higher (about 2%) than the experimental values. The calculated values obtained for unstable single-phase β as the reference state are slightly lower (1 to 2%) than the experimental values. It should be noted that the enthalpy obtained with unstable single-phase β as the reference state consists only of the contribution of the pure elements in the β structure since the temperature-independent parameter is eliminated. If an excess term is introduced to fit the experimental specific heat capacity data exactly, this discrepancy would be even more pronounced.

The lattice parameters of Ti-rich β_1 and Nb-rich β_2 in the metastable two-phase equilibrium (no α) should differ by, at least, 0.001 nm [14]. Thus, X-ray diffraction (XRD) experiments should be able to discern the presence of the two phases. X-ray analysis was done on heat-treated specimens. These specimens were pulse-heated to 2085 K, held steady at this temperature for 1 s, and allowed to cool naturally inside the chamber. This is essentially the same heat treatment imparted to specimens used for the thermophysical property measurements. The XRD results show that at this cooling rate, single-phase β is retained at room temperature. The lattice parameter determined from this analysis is (0.3292 ± 0.0002) nm. This value is noticeably larger than the values summarized by Murray [14] for retained single-phase β of this composition (0.3285 nm). Although the absorption of interstitial elements, such as oxygen, in pure Ti can result in an increase in the lattice parameter, an improbably high concentration of interstitial element (>3 atom%) throughout the sample's radius would be required to account for the larger lattice parameter. Such contamination of the sample is unlikely, since the heat treatment was carried out in an argon atmosphere and the predicted diffusion length for the heat-treatment duration (1 s) and relevant length scale (1 mm) would require a diffusion constant of 10^{-2} cm$^2 \cdot$ s^{-1}, three orders of magnitude greater than even liquid diffusion constants. In order to support this assumption, another sample was heat-treated for 1 s at 1530 K. The XRD result of this sample also showed a single-phase β, with a lattice parameter of 0.3291 ± 0.0002 nm. Since contamination is considered to be highly unlikely and the alloy composition was verified [10], no explanation for this larger lattice parameter

could be found. It can, however, be concluded that the initial condition of the specimen before the experiments consisted of unstable single-phase β or metastable two-phase ($\beta_1 + \beta_2$) but not equilibrium ($\alpha + \beta$).

7. CONCLUSION

The present work validates the applicability of the laser polarimetry technique to the determination of thermophysical properties of alloys. The experimentally determined values for the specific heat capacity and enthalpy of the 53Nb–47Ti (mass%) alloy were shown to agree within 2% with those computed from a thermodynamic model of the Nb–Ti system. In addition, the current study illustrates a few additional considerations associated with the property determination of alloys, as opposed to pure metals. Experimentally determined properties of alloys are dependent on their state prior to the experiments. For alloys having phase transformations in or below the temperature range of interest, the initial room temperature phase and microstructure may be altered during the pretreatment, pulse experiment, or subsequent cooling, depending on the characteristics of the transformation kinetics. For such alloys, care should be taken to identify properly the initial state of the alloy prior to the experiments and to impart any heat treatment necessary to achieve the desired initial phase and microstructure, as the enthalpy has been shown to be dependent on the reference state.

ACKNOWLEDGMENT

We thank W. J. Boettinger for his valuable advice and suggestions regarding this paper.

REFERENCES

1. A. Cezairliyan, M. S. Morse, H. A. Berman, and C. W. Beckett, *J. Res. Natl. Bur. Stand. (U.S.)* **74A**:65 (1970).
2. A. Cezairliyan, *J. Res. Natl. Bur. Stand. (U.S.)* **75C**:7 (1971).
3. S. Krishnan, *J. Opt. Soc. Am.* **A9**:1615 (1992).
4. A. Cezairliyan, S. Krishnan, and J. L. McClure, *Int. J. Thermophys.* **17**:1455 (1996).
5. A. Cezairliyan, S. Krishnan, D. Basak, and J. L. McClure, *Int. J. Thermophys.* **19**:1267 (1998).
6. A. Cezairliyan, *Int. J. Thermophys.* **4**:159 (1983).
7. E. Kaschnitz and A. Cezairliyan, *Int. J. Thermophys.* **17**:1069 (1996).
8. A. Cezairliyan, G. M. Foley, M. S. Morse, and A. P. Miiller, *Temperature—Its Measurement and Control in Science and Industry*, *Vol. 6*, J. F. Schooley, ed. (AIP, New York, 1992), pp. 757–762.

9. T. Matsumoto and A. Cezairliyan, *Int. J. Thermophys.* **18**:1539 (1997).
10. D. Basak, W. J. Boettinger, D. Josell, S. R. Coriell, J. L. McClure, S. Krishnan, and A. Cezairliyan, *Acta Met.* **47**:3147 (1999).
11. K. C. Hari Kumar, P. Wollants, and L. Delaey, *CALPHAD* **18**:71 (1994).
12. A. T. Dinsdale, *CALPHAD* **15**:317 (1991).
13. D. L. Moffat and U. R. Kattner, *Metall. Trans.* **19A**:2389 (1988).
14. J. L. Murray, *Phase Diagrams of Binary Titanium Alloys*, J. L. Murray, ed. (ASM International, Metals Park, OH, 1987), p. 188.